17th AIAA/CEAS Aeroacoustics Conference (32nd AIAA Aeroacoustics Conference)
05 - 08 June 2011, Portland, Oregon

AIAA 2011-2897

A New Modular Fan Rig Noise Test and Radial Mode Detection Capability

Ulf Tapken, Roland Bauers and Lars Neuhaus
German Aerospace Center (DLR), Institute of Propulsion Technology, Engine Acoustics Branch, Berlin, Germany

Nick Humphreys, Alec Wilson
Rolls-Royce, Derby, UK

Christian Stöhr
Rolls-Royce Deutschland, Dahlewitz, Germany

Matthias Beutke
AneCom AeroTest GmbH, Wildau, Germany

A new major large-scale fan rig test facility, UFFA (Universal Fan Facility for Acoustic), has been designed with the objective to allow test bed changes for engine representative OGVs and bypass duct annulus and liners, for reduced build times, and higher fidelity investigation of aft fan noise technologies. An important enhancement consisted in the implementation of three Radial Mode Detection (RMD) devices in the bypass duct and further downstream in the nozzle equivalent plane. High effort was spend on the realisation of a wall-flush mounted sensor array, which has the advantage not to disturb the flow and the acoustic field. However, the separation of different radial mode contributions is realised only implicitly by the analysis of the axial wave number spectrum, which is particularly challenging if sensors are installed only at the outer duct wall. More robust from the numerical point of view is the established technique to directly measure the radial structure of the sound field with sensor rakes. It is one of the main objectives of this paper to verify whether both techniques deliver the same experimental results also at the high targeted frequencies up to kR=75. As the examination of recently obtained data revealed, the sensor rake measurements were influenced by aerodynamic perturbations originating from the fan rotor wakes. The radial mode analysis could be significantly improved by incorporation of appropriate aerodynamic eigenfunctions. Further investigated was the sensitivity of mode detection with sensor rakes against manufacturing and installation tolerances.

I. Introduction

A major new large scale fan rig test facility, UFFA (Universal Fan Facility for Acoustic), has been designed, manufactured and commissioned by AneCom AeroTest GmbH, Wildau, Germany. The new modular fan rig test facility builds on previous Rolls-Royce large scale fan rig design experience[1] but extends the experimental capability to allow test bed changes for engine representative OGVs and bypass duct annulus and liners, for reduced build times, and higher fidelity investigation of aft fan noise technologies. In order to meet the challenging noise targets in a timely manner for future aircraft, the industry requires engine and nacelle representative high Technology Readiness Level validation test vehicles to deliver the technology ready for implementation in to the full scale product.

An important enhancement consisted in the implementation of three Radial Mode Detection (RMD) devices in the bypass duct, i.e. radial sensor rakes directly at OGV exit and radial sensor rakes respectively a wall-flush mounted sensor array further downstream in the nozzle equivalent plane of the UFFA test facility. The sensor arrays were developed by DLR within the frame of the EU FP 6 project VITAL[2], based on predicted sound field characteristics provided by Rolls-Royce. At the maximum targeted frequency of kR=75 more than 2500 modes of azimuthal mode orders up to m=85 and radial mode orders up to n=10 should be resolved. Major objectives of future RMD measurements are (1) the accurate assessment of fan rig design changes, (2) the provision of high quality data

American Institute of Aeronautics and Astronautics

for the validation of CFD or CAA calculations and (3) the provision of mode amplitudes as input for far-field radiation prediction codes.

High effort was spend on the realisation of the wall-flush mounted sensor array, which has the advantage not to disturb the flow and the acoustic field. However, the separation of different radial mode contributions is realised only implicitly by the analysis of the axial wave number spectrum, which is particularly challenging if sensors are installed only at the outer duct wall[3]. More robust from the numerical point of view is the established technique to directly measure the radial structure of the sound field with sensor rakes[4,5]. It is one of the main objectives of this paper to compare the experimental results achieved with both techniques. So far this was accomplished only at very low frequencies[6].

At the targeted high frequencies the sound field exhibits a fine spatial structure. During the design of the sensor rakes the question emerged, how sensitive the mode detection is against tolerances with respect to rake manufacturing and installation. The impact was studied by means of simulated measurements with systematic variation of the assumed and the actual sensor midpoints.

Another issue investigated in the present paper is the influence of aerodynamic waves on the radial mode decomposition. Significant pressure fluctuations are produced in particular by the rotor wakes, which are partly scattered at the stator vanes, travel downstream with nearly mean flow velocity and superpose the measured acoustic field. A first attempt to improve the quality of the mode detection consists in the incorporation of an aerodynamic model. This approach was devised and successfully demonstrated during the analysis of a CFD calculation by Weckmüller et al[7].

II. Overview of Fan Rig

The new fan rig, UFFA, is of a modular construction that allows rapid test bed changes to the total LP fan system including the intake, fan, outlet guide vanes (OGVs) and bypass duct. Additionally the bypass – core splitter and engine section stators may also be replaced. The requirement specification of the fan rig produced by Rolls-Royce allows turbofan powerplant fan, OGV, annulus lines and acoustic liners to be replicated. Maintaining the large scale of the fan rig[1] allows engine, duct and acoustic liner components to be tested with confidence with regard to their performance at full scale. The modular fan rig fan diameter is 34 inches and is powered by an 18MW Motor. The noise instrumentation standard of previous Rolls-Royce fan rigs[1] has been maintained including 3 non equi spaced circumferential mode detection arrays developed previously by NLR[8], and extended by means of a 180 microphone Rotating Microphone Array (RMA) downstream of the engine style bypass duct section. The RMA will be the subject of a future paper. Farfield measurements within the AneCom AeroTest facility are also undertaken within the anechoic chamber for inlet propagating noise[9].

Fig. 1: UFFA rig installed in the anechoic test facility of AneCom AeroTest.
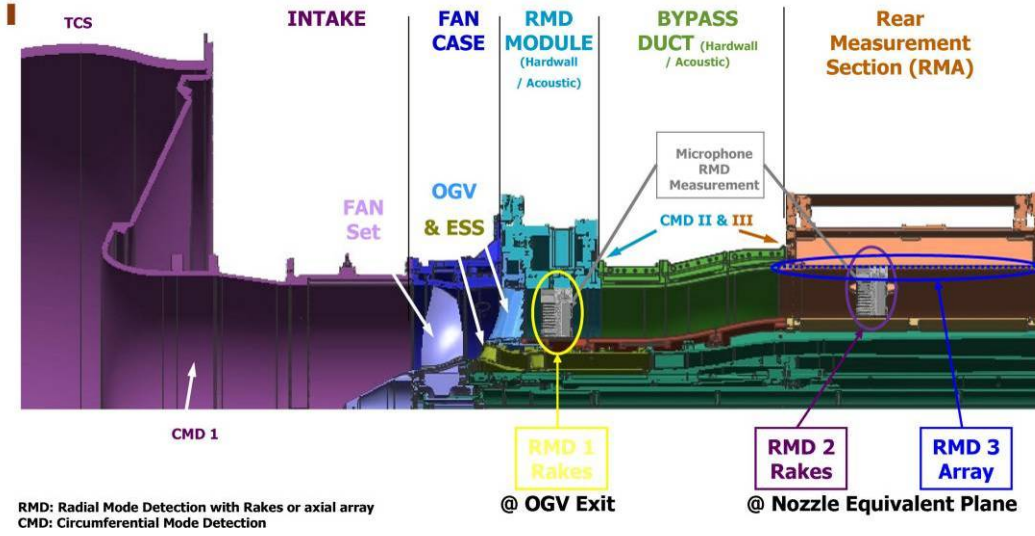
Fig. 2: Sectional view of UFFA rig.

III. Outline of inverse radial mode detection technique

Radial mode analysis (RMA) is an experimental technique that delivers the complex amplitudes of higher order acoustic modes propagating up- and downstream in flow ducts of e.g. turbo machinery. It is based on the analytical description of the in-duct sound propagation in the frequency domain. Under the constraints of incompressible and isentropic flow, constant axial mean flow profile, stationary mean temperature and density, the solution of the convective Helmholtz equation is given in cylindrical coordinates by a linear superposition of modal terms[10] as follows:

$$p(x,r,\varphi) = \sum_{m=-\infty}^{\infty} \sum_{n=0}^{\infty} \left(A_{mn}^{+} \cdot e^{ik_{mn}^{+}x} + A_{mn}^{-} \cdot e^{ik_{mn}^{-}x} \right) \cdot f_{mn}(r) \cdot e^{im\varphi} \ . \tag{1}$$

Here k_{mn}^{+} and k_{mn}^{-} denote the axial wave numbers, A_{mn}^{+} and A_{mn}^{-} the complex amplitudes of the mode with the azimuthal order m and the radial order n for propagation in and against flow direction, respectively. In the case of hard-walled acoustic boundary conditions, the modes form an orthogonal eigensystem. The modal shape factors are given by $f_{mn}(r) = (F_{mn})^{-\frac{1}{2}} (J_m(\sigma_{mn}r/R) + Q_{mn}Y_m(\sigma_{mn}r/R))$, with J_m and Y_m being the Bessel functions of first and second kind and order m with associated hard-walled cylindrical eigenvalues σ_{mn} and Q_{mn}. The eigenvalues depend on the hub-to-tip ratio η. Q_{mn} is zero for non-annular cylinders; R is the outer duct radius. The definition of the normalization factor F_{mn} is given in Ref.[3].

In a hard walled duct the sound power is only transported in axial direction. The sound power carried by each individual mode can be calculated according to Morfey[11] as

$$P_{mn}^{\pm} = \frac{\pi R^2}{\rho c} \frac{\alpha_{mn}(1-M^2)^2}{(1\mp\alpha_{mn}M)^2} \left| A_{mn}^{\pm} \right|^2 \ . \tag{2}$$

with $\alpha_{mn} = (1-(1-M^2)(\sigma_{mn}/(kR))^2)^{\frac{1}{2}}$. For a better identification of the sound generation mechanisms, in some cases it is useful to sum up the sound power of the individual radial modes for each azimuthal mode order, i.e. $P_m^{\pm} = \sum_n P_{mn}^{\pm}$.

The determination of the radial mode spectrum can be regarded as an inverse problem, i.e. the solution is deduced by means of an inversion of the matrix $\mathbf{W}$ relating a vector $\mathbf{p}$ of measured complex sound pressure values to a vector $\mathbf{A}$ of radial mode amplitudes: $\mathbf{p} = \mathbf{W}\,\mathbf{A}$. In most applications, this system has more parameters than unknowns. A linear least squares fit, e.g. by deploying the pseudo-inverse of matrix $\mathbf{W}$, can be used to determine the radial mode amplitudes:

$$\mathbf{A} = [\mathbf{W}^{H}\mathbf{W}]^{-1}\mathbf{W}^{H}\,\mathbf{p}. \tag{3}$$

The resulting mode amplitude vector minimizes the cost function J = ||**e**|| = ||**WA** − **p**||, where || || denotes the 2-norm. The complex vector of errors **e** represents noise due to e.g. turbulent pressure fluctuations as well as an inappropriate description of the mode propagation in the flow duct by the utilized analytical model.

As discussed in detail by Nelson and Yoon[12], the solvability and stability of matrix Eq. (3) as well as the sensitivity of the system against noise is related to the condition number of the model matrix $\kappa(\mathbf{W})$. In general, the matrix condition mainly depends on various parameters: the frequency kR, the cut-on mode orders m and n, the duct hub-to-tip ratio, the mean flow parameters and the chosen measurement positions[3]. The condition number is defined as the ratio of the maximum to the minimum singular value, which can be derived from the singular value decomposition (SVD) of W[12].

Since the condition number is only a global quantity defining an upper bound, the propagation of small measurement inaccuracies into the radial mode amplitudes is further investigated by means of a computer simulation. Generally, measurement inaccuracies have systematic as well as stochastic sources. Here, only the influence of a stochastic type of an error source is considered. The noise amplitude is assumed to be the superposition of several independent stochastic noise sources, the distribution of which can be described in good agreement by a Gaussian distribution. The implementation of the simulation is shown schematically in Fig. 3 and described in detail in reference[3]. By carrying out N_{avg} simulated sound pressure measurements with the given standard deviation s_p at all positions of the measurement grid, the standard deviation s_{mn} of the indididual mode amplitudes can be assessed. Further, a quantity representing the overall amplification of the measurement uncertainties inherent to the solution eq. (3) can be calculated

$$A_{mn,rel} = \frac{\left\|\tilde{A}_{mn}\right\|\|p\|}{\|A_{mn}\|\|\tilde{p}\|},$$ (4)

for which $\|A_{mn,rel}\| \leq \kappa(\mathbf{W})$ holds.

In specific applications the matrix condition and thus the analysis quality can be substantially improved by the application of regularization techniques, as e.g. was intensively investigated by Kim and Nelson[13].
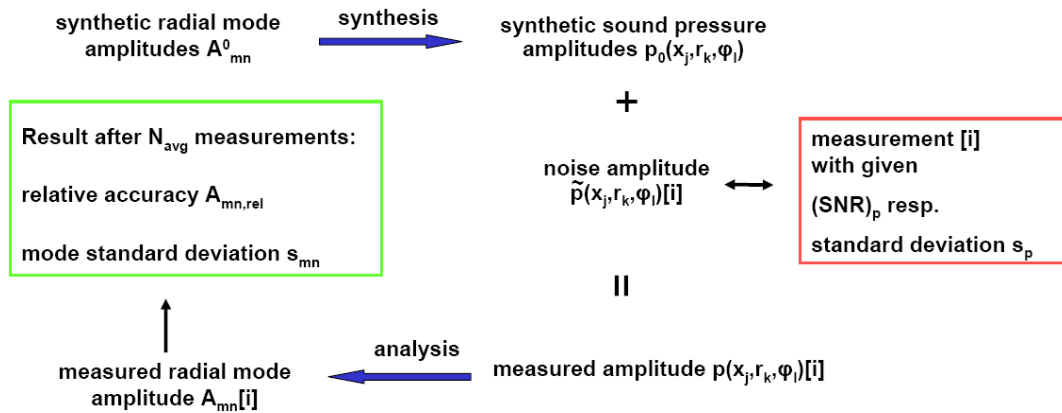
synthetic radial mode amplitudes A^0_{mn} — synthesis → synthetic sound pressure amplitudes $p_0(x_j, r_k, \varphi_l)$

Result after N_{avg} measurements:

relative accuracy $A_{mn,rel}$

mode standard deviation s_{mn}

+

noise amplitude $\tilde{p}(x_j, r_k, \varphi_l)[i]$ ↔ measurement [i] with given $(SNR)_p$ resp. standard deviation s_p

=

measured radial mode amplitude $A_{mn}[i]$ ← analysis — measured amplitude $p(x_j, r_k, \varphi_l)[i]$

Fig. 3: Simulation scheme for the assessment of the propagation of measurement noise into the radial mode amplitude spectrum.

IV. Design of sensor arrays for radial mode detection in the bypass duct

Mode measurements were envisaged at two stations: the first directly downstream of the OGV exit and the second in a nozzle equivalent plane. The left diagram in Fig. 4 depicts the azimuthal and radial mode orders that are able to propagate in the BPD duct at a particular operating condition. At the upper frequency corresponding to $kR = 75$ more than 2500 modes are propagating in the mode analysis duct section, whereby the maximum azimuthal mode order is $m = \pm 85$ and the maximum radial mode order is $n = 10$.

Several array variants with different numbers and positions of sensors were studied by analyzing the condition of the model matrix $\kappa(\mathbf{W})$. The configurations did comprise microphones either mounted in radial rakes or flush mounted on the outer duct wall and were optimised with respect to maximum frequency, required axial length of the duct section, number of data acquisition channels, measurement time and hardware costs. For illustration Fig. 5

shows the variation of the RMD numerical condition for analysis of mode m = 0, which is most difficult to analyse, with frequency and axial sensor separation. For the case depicted in the left diagram rakes in two axial planes with 11 radially distributed sensors and for the case depicted in the right diagram an axial array of 60 microphones flush mounted at the outer duct wall were assumed.

The sensor configurations that were finally selected comply with the design guidelines given in Ref.2 and are depicted in Fig. 6. They have following specifications:

- RMD1 at the OGV exit: consisting of 12 sensor rakes installed in a rotatable duct section in N_x=2 axial planes with separation $\Delta x \approx 0.031R$, all rakes with equidistant azimuthal spacing and axially alternating, each rake holding Nr=11 microphones
- RMD2 in the nozzle equivalent plane: consisting of 6 sensor rakes installed in a rotatable duct section in N_x=2 axial planes with separation $\Delta x \approx 0.0265R$, all rakes with equidistant azimuthal spacing and axially alternating, each rake holding Nr=11 microphones
- RMD3 in the nozzle equivalent plane: consisting of 3 azimuthally staggered axial arrays each with N_x=60 microphones mounted with axial separation $\Delta x \approx 0.0275R$ flush with the outer duct wall, installed in the same rotatable duct section as RMD2.

For all arrays 1/4" high quality condenser microphones were used. The rake microphones are equipped with nose cones, point upstream and are installed in aerodynamically shaped rake bodies. Rake body vibrations were investigated numerically and were proven to be sufficiently weak. The length of the wall-flush mounted axial array is $L_x = (N_x-1) \Delta x \approx 1.6225R$.
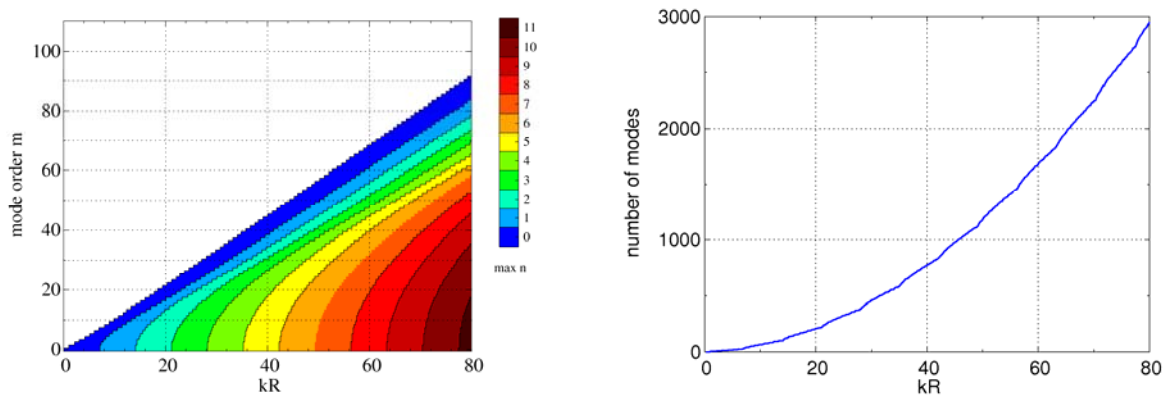

Fig. 4: Azimuthal and radial mode orders (left) respectively total number of modes (right) that are able to propagate in the BPD nozzle equivalent plane.
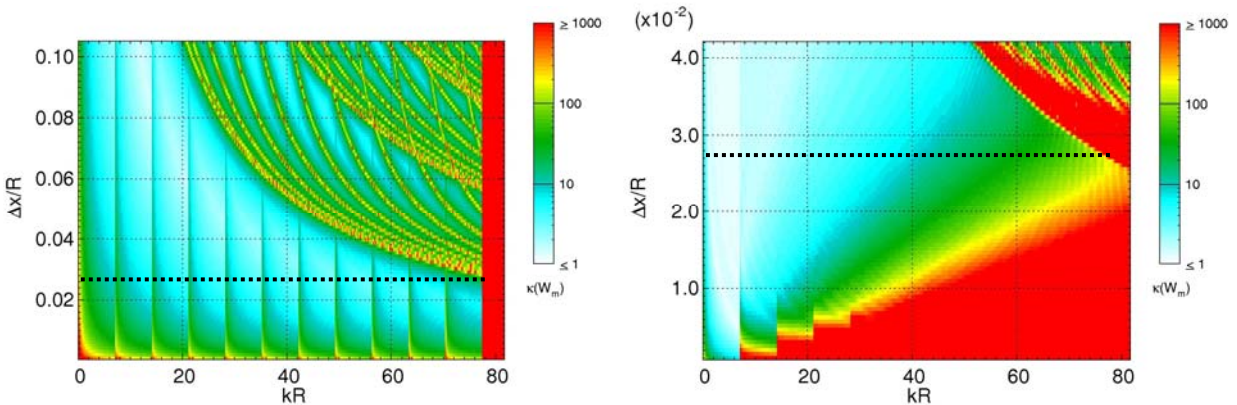

Fig. 5: Condition analysis of model matrix W for radial mode decomposition of mode order m=0 using radial sensor rakes (left) respectively a wall-flush axial sensor array (right) with variable sensor spacing Δx.

American Institute of Aeronautics and Astronautics

Fig. 6: Sensor rakes RMD1 at OGV exit (left photo). Sensor rakes RMD2 and axial sensor array RMD 3 at nozzle equivalent plane.

V. Analysis of sound pressure time series

Radial mode detection measurements were carried out by rotating the respective instrumented duct section in steps of 2 deg to obtain regular data grids. Consequently, with RMD2 and RMD3 grids consisting of 3960 respectively 10800 positions were achieved. The standard measurement duration was 15s, the data were acquired with up to 48 kHz sampling frequency and 24-bit resolution.

The analysis of the measured sound pressure time series consisted of two subsequent steps: The first step was to perform a so-called 'adaptive resampling' process, in which the sampling frequency was adaptively corrected with respect to speed variations of the fan shaft. This required the recording and analysis of a 'one-pulse-per-revolution'-signal of the rotor shaft. In the second step, the Fourier transforms of the sound pressure time series were calculated for all measurement points. The effect is exemplarily depicted in Figures Fig. 7 and Fig. 8. Shown are the mean auto-power spectrum and the mean sound pressure spectrum achieved with adaptive resampling, respectively. For RMD3 the averaging was carried out over all available 10800 positions, for RMD2 all spectra measured at radial position r=1, i.e. only 360 positions closest to the duct wall, were averaged. Due to the adaptive resampling process the spectral components are a function of the engine order. The spectrum demonstrates that all portions of the sound field not fully correlated with the shaft speed are suppressed effectively.

For the fan rig configuration treated in this paper, at 50% shaft speed the BPF and 2BPF components hardly protrude from the overall noise floor. For BPF the rotor-stator interaction modes are cut-off at the given operating condition. 2BPF is strongly affected by an acoustic liner located in the bypass duct upstream of the RMD2 and RMD3 measurement sections. At 100% shaft speed the BPF component is still weak due to the acoustic liner. However, at radial station r=1 of the RMD2 rakes the BPF-level is much stronger compared to the RMD3 measurement, which according to the investigations of section VIII presumably can be ascribed to superposed hydrodynamic modes.

In order to evaluate the impact on the mode detection accuracy, the uncertainty of the sound pressure measurement was assessed systematically by calculating the sound pressure standard deviation with application of the procedure described in reference[14]. The standard deviation is depicted in Figures Fig. 9 and Fig. 10 for various measurement durations represented by the number of applied FFT-windows N_{win}. For the statistical analysis time series of up to 120s length were acquired for a small sub-set of traversing positions. Using 50% FFT-overlap, the standard acquisition time of 15 s corresponds corresponded approximately to N_{win} = 42. It should be noted that for RMD2 data of all radial positions was evaluated.

At 50% shaft speed the signal-to-noise ratio is quite low for BPF due to the cut-off design of the fan. As already observed in Fig. 7, compared to RMD3 the average SPL measured by RMD2 is larger due to the hypothetical hydrodynamic modes.

At higher frequencies corresponding to higher BPF-harmonics and increased shaft speeds the signal-to-noise ratio is much larger, which is due to the less effective acoustic liner but also allows the conclusion that the flow conditions of the rig were excellent and thus the aeroacoustic source mechanisms undisturbed.
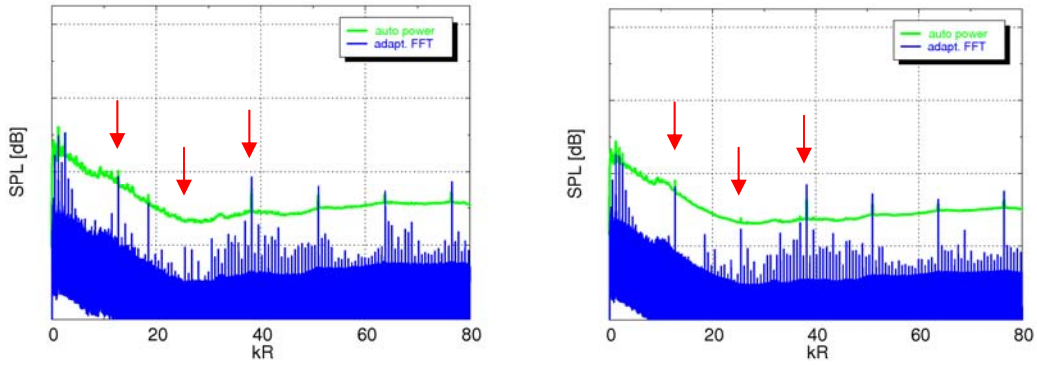
Fig. 7: Mean auto-power spectrum and mean rotor-coherent sound pressure spectrum after application of adaptive resampling measured with RMD2 (left) and RMD3 (right) at 50% shaft speed (BPF, 2BPF and 3BPF marked by red arrows).
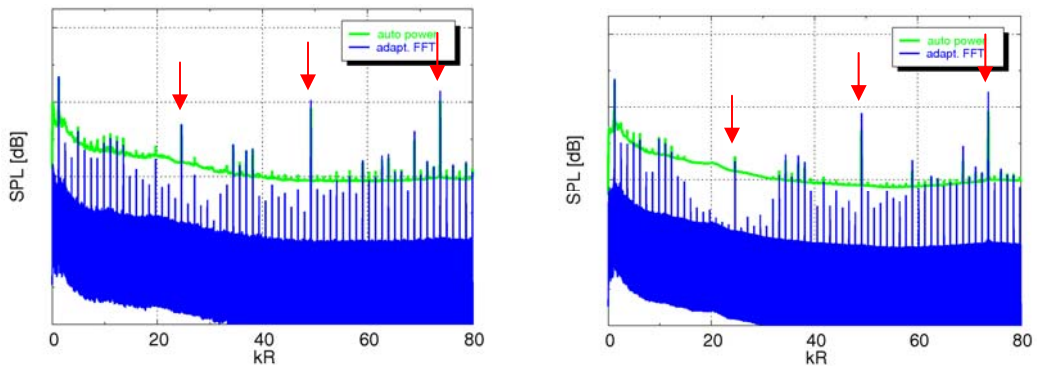
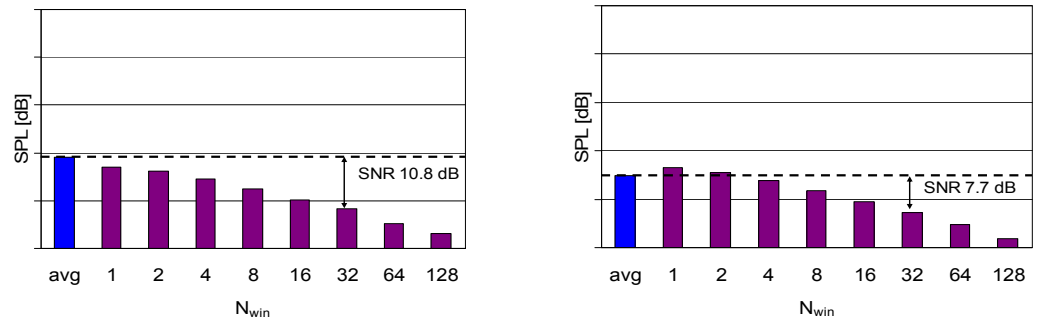

Fig. 8: Same as Fig. 7 but at 100% shaft speed.

Fig. 9: SPL of average sound pressure (blue bar) and standard deviation (violett bars) calculated for variable measurement duration corresponding to N_{win}. The left and right diagram were calculated for RMD2 respectively RMD3 analysis of BPF at 50% shaft speed.
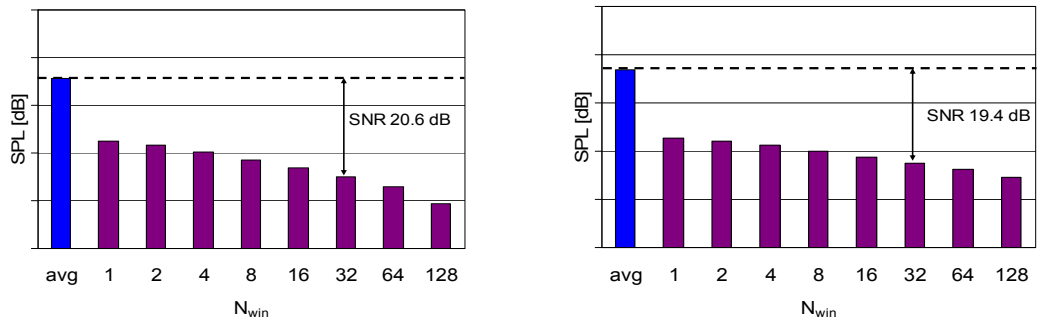
Fig. 10: Same as Fig. 9 but for 3BPF at 80% shaft speed.

American Institute of Aeronautics and Astronautics

VI. Mode detection accuracy of radial sensor rakes RMD2 and wall-mounted array RMD3

For all investigated operating conditions the sound fields of the BPF harmonics were decomposed into the individual radial modes by application of Equation (3). The input vector comprised the complex sound pressure values obtained with arrays RMD2 or RMD3 at the 3960 respectively 10800 grid positions. In the standard analysis procedure only acoustic cut-on mode orders were taken into account. Further a mean axial flow profile independent of the radial coordinate was assumed. It should be noted that both arrays were measured separately, e.g. RMD3 was measured with RMD2 rakes removed.

In section IX it will be verified that both arrays RMD2 and RMD3 measure the same dominant mode orders and thus deliver comparable results. However, when looking more into the details of the mode spectra, some differences can be found. These are related to some extent to the differing sensor placements and will be illustrated in the following.

Fig. 11 shows typical results measured with both arrays for 3BPF at 80% shaft speed. Depicted are the amplitudes of all radial modes, which propagated downstream and upstream in the measurement duct. To enable a visual comparison an identical logarithmic color scaling was chosen. Further, the same data set is shown in Fig. 25 in another representation, i.e. the sound power transported by the individual azimuthal orders, which allows a better identification of the generating mechanisms.

The outcome of both RMD measurements is that $m=18$ is the most dominant rotor-stator interaction mode order. A more detailed look reveals that according to RMD2 measurement most energy is concentrated in the lowest radial constituent $(18,0)$, whereas the outcome of RMD3 is that modes $(18,0)$, $(18,1)$ and $(18,2)$ contribute almost equally. Generally the expectation is that with the RMD2 rakes the radial structure of the modes is detected in a more accurate way compared to the indirect measure at the duct wall via an implicit axial wave number analysis. The second largest mode order is $m=-24$, for which both arrays measure strongest contributions from the three lowest radial orders, but with slightly higher amplitudes assessed by RMD2. Next dominant mode orders are $m=-19$, $m=19$ and $m=23$, for which no explanation could be found yet. They are detected by RMD2 and RMD3 with different levels. Mode $m=16$ was captured with significant level, but by RMD3 only.

Further noticeable are for RMD3 above-average noise levels of modes with azimuthal orders $-20 \leq m \leq 20$ and radial mode orders $0 \leq n \leq 2$. These follow from the numerical properties of the model matrix, as the analysis of error propagation in Fig. 12 shows. Depicted are the standard deviations of all mode orders for RMD2 and RMD3 in comparison. They were calculated according to the scheme described in section III and with application of the specific signal-to-ratios evaluated in Fig. 10. The characteristic increase of mode standard deviations for the wall-flush mounted RMD3 array can be ascribed to the fact that for high frequencies the cut-on ratios and with this the axial wave numbers become quite similar, so that in the implicit wave number analysis modes of equal azimuthal and different low radial order cannot be distinguished properly.

On the other hand for array RMD2 the major drawback is related to the analysis of modes close to cut-off, see the left diagram in Fig. 12. Modes close to cut-off exhibit very high axial phase speeds and thus hardly can be captured by measurements in two planes with small axial separation. The increased modal noise levels are also visible in Fig. 11.

Despite the fact that for both arrays RMD2 and RMD3 the deduced mode standard deviations are estimated to small, they in principle reflect the modal domains of increased noise levels. It is important to keep in mind that the described mode standard deviations represent only the lower estimate of inaccuracies mapped from the measured sound pressure standard deviation in the analysis process:

- fluctuations of the coherent aeroacoustic source mechanisms e.g. due to shaft speed variations,
- contributions of incoherent aero-acoustic sources,
- turbulent pressure fluctuations and
- noise components of the electronic measurement hardware.

Not included are shortcomings of the model underlying the mode analysis with regard to

- three dimensional characteristics of the flow field (e. g. temporal or spatial gradients, influence of EGV wakes),
- dimensional tolerances of the rig itself or
- dimensional tolerances of the microphone positions.

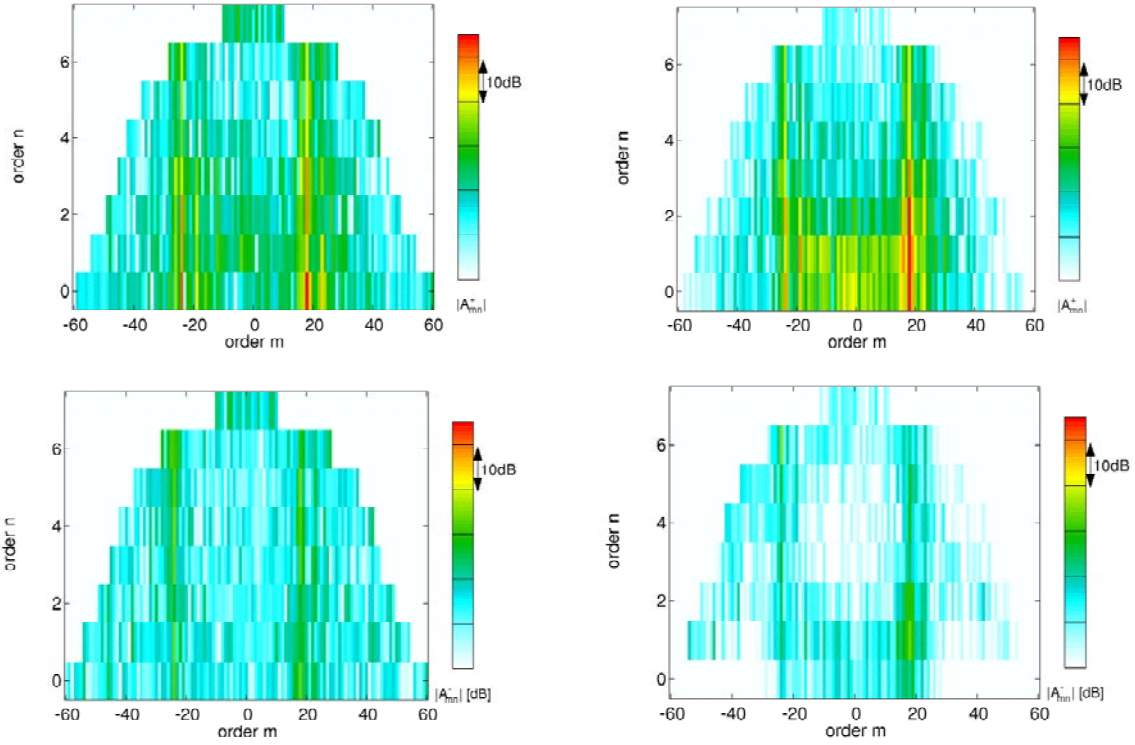American Institute of Aeronautics and Astronautics

Fig. 11: Amplitudes of the downstream (top) and the upstream (bottom) propagating modes measured by RMD2 (left) and RMD3 (right) for 3xBPF at 80% shaft speed.
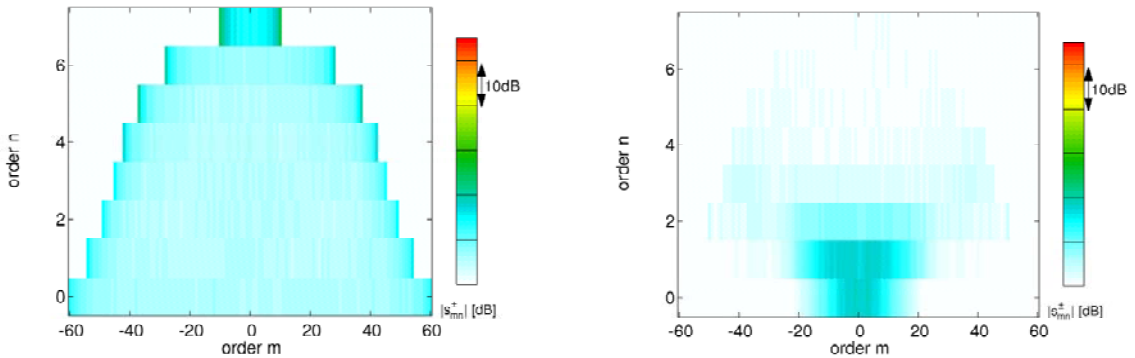

Fig. 12: Standard deviation of the individual mode amplitudes measured by RMD2 (left) and RMD3 (right) for 3xBPF at 80% shaft speed.

Moreover, the described error propagation characteristics are valid for all frequencies of interest, as can be verified in Fig. 13. Depicted in Fig. 14 is the quantity $A_{mn,rel}$ from equation (4), which describes the overall amplification of uncertainties connected with the mode decomposition of individual azimuthal mode orders. In the left diagram calculated for the RMD2 sensor rakes, the cut-on-frequencies of the radial mode orders that are connected with increased errors are clearly visible. Apart from this, according to this study radial mode analysis is feasible in the whole frequency range with good accuracy.

The characteristic of the wall-mounted array RMD3 is totally different. The amplification of measurement perturbations is generally weaker for frequencies below kR=40. For higher frequencies this is still true for azimuthal mode orders |m|>20. For lower azimuthal mode orders however, the accuracy is expected to be inferior because of the larger radial mode content and in particular the converging cut-on ratios. Above the maximum target frequency of kR=75 no radial mode decomposition is not feasible. It should be noted that all results were computed without application of regularization techniques.
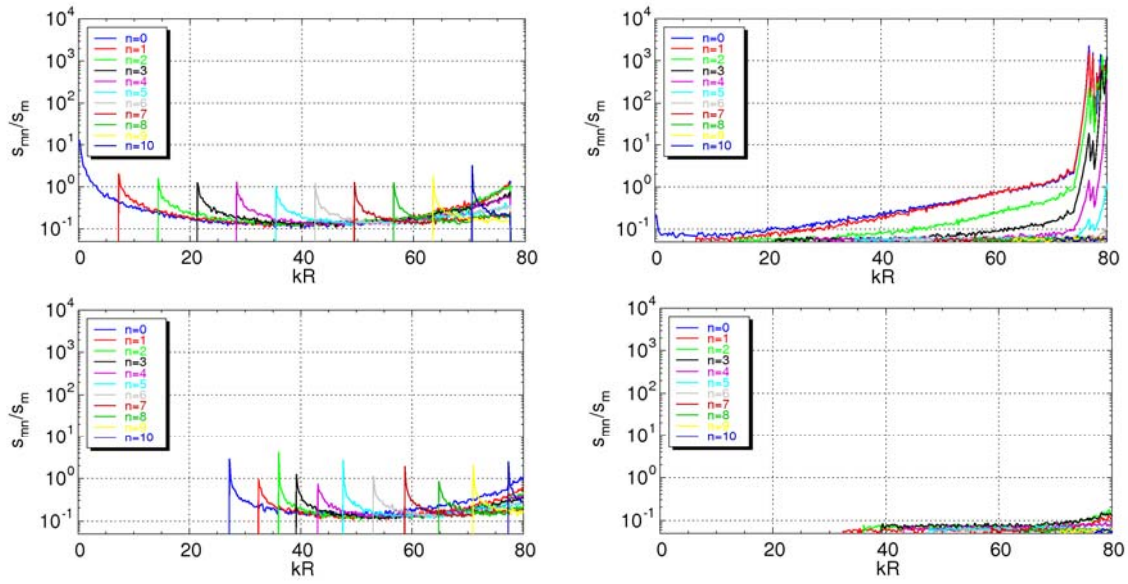
American Institute of Aeronautics and Astronautics

Fig. 13: Mode standard deviation for the radial mode decomposition of mode order m=0 (top row) and m=30 (bottom row) with sensor arrays RMD2 (left column) and RMD3 (right column) at variable frequency.
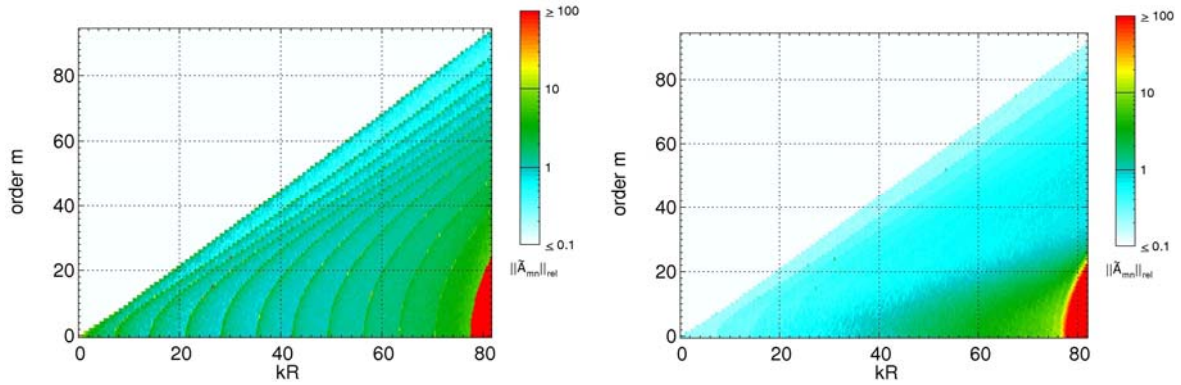

Fig. 14: Overall accuracy of the radial mode decomposition of mode order m with sensor arrays RMD2 (left) and RMD3 (right) at variable frequency.

VII.   RMD sensitivity against tolerances in sensor rake manufacturing and installation

The impact was evaluated by means of simulated radial mode measurements with the assumption that one out of 12 sensor rakes is displaced in the axial, radial or azimuthal coordinate relative to the assumed measurement positions. With regard to the practical installation of the rake, the impact of rake tipping in the r-φ plane, rake tipping in the x-r plane and rake rotation around the shaft axis was also considered. The table and sketches in Fig. 15 show the definitions and the interrelations of different sensor rake displacements and associated displacements of the sensor membrane in the cylinder coordinate system. The simulations were carried out for the RMD1 rakes and synthetic sound fields with equal mode amplitudes for the downstream respectively upstream propagating modes: $|A^+_{mn}|$=85 dB, $arg(A^+_{mn})$=random(0,2π) and $|A^+_{mn}|$=75 dB, $arg(A^+_{mn})$=random(0,2π).

In contrast to section VI here the influences of systematic errors are investigated. Measure for the impact of the installation imprecision is the difference between analysed and synthetic mode amplitudes evaluated for 150 repeated analyses of different random sound fields. The results depicted in Fig. 16 for frequency kR=60 show different typical signatures. The relative amplitude scaling is the same as was used in Fig. 11 and Fig. 12 but with an offset of -20dB. An axial misalignment leads to larger deviations for low mode orders (m,n) and modes close to cut-off. A rotation of the rake around the shaft axis mainly causes circumferential offsets, which causes large deviations mainly for modes close to cut-off. Realistic radial displacements have minor consequences.

In Fig. 17 the impact of axial offset, radial offset and rotation around the shaft axis on the overall RMD accuracy are shown for various frequencies. For comparison the result of a measurement using the correct sensor positions but with superposed noise of signal-to-ratio SNR_p=25dB is shown. It is expected, that for the whole sensor rake arrangement installed in the MFR the tolerances impact of all twelve rakes effectively will be larger, i.e. the present results can be regarded as lower bound for the resulting RMD inaccuracies.

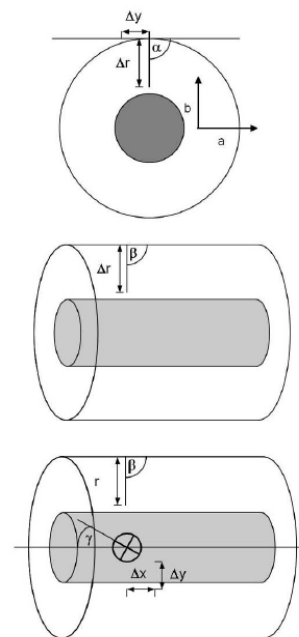| Displacement of sensor rake shaft		Displacement of sensor membrane position		
		Δx [mm]	Δr [mm]	Δφ [°]
axial offset Δx [mm]	± 0.4	± 0.4		
	± 0.8	± 0.8		
radial offset Δr [mm]	± 0.15		± 0.15	
	± 0.3		± 0.3	
tangential offset Δy [mm]	± 0.4		< 0.001	±0.09 … ±0.06
	± 0.8		+ 0.001	±0.17 … ±0.11
tipping in r-φ plane α [°]	0.3		0.003 … 0	-0.18 … -0.01
	0.6		0.014 … 0.001	-0.37 … -0.02
	0.9		0.032 … 0.002	-0.55 … -0.03
tipping in x-r plane β [°]	0.3	-0.84 … -0.08	0.35 … 0.34	
	0.6	-1.68 … -0.15	0.69 … 0.69	
	0.9	-2.52 … -0.22	1.05 … 1.03	
rotation around rake shaft axis γ [°]	0.3	< 0.001	< 0.001	0.07 … 0.05
	0.6	≈ 0.004	< 0.001	0.15 … 0.10
	0.9	≈ 0.008	< 0.003	0.22 … 0.14

Fig. 15: Definition of potential rake shaft displacements due to installation tolerances. For some rake shaft displacements different membrane displacements results at radial sensor position r=11 (close to the hub) ...r=1 (close to the outer duct wall).
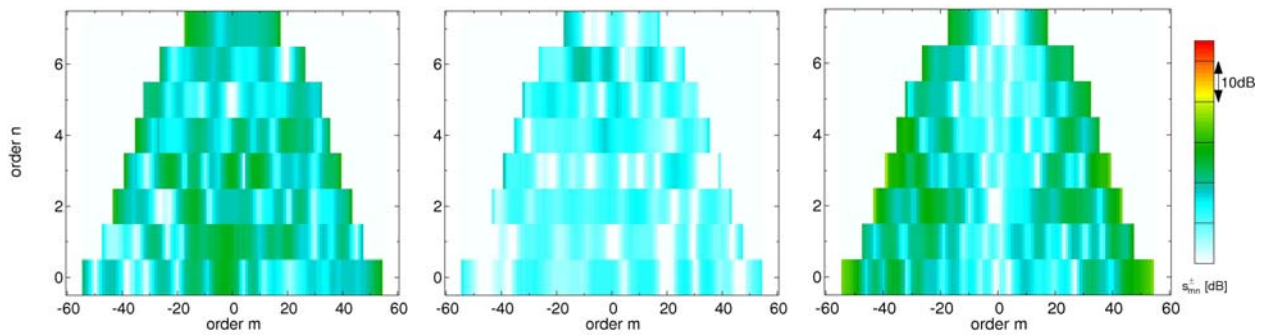
Fig. 16: Impact of RMD1 sensor rake installation tolerances on standard deviation of mode amplitudes at frequency kR=60 (from left to right: rake axial offset Δx=-0.8mm, rake radial offset Δr=0.3mm, rake shaft rotation γ=0.9°)
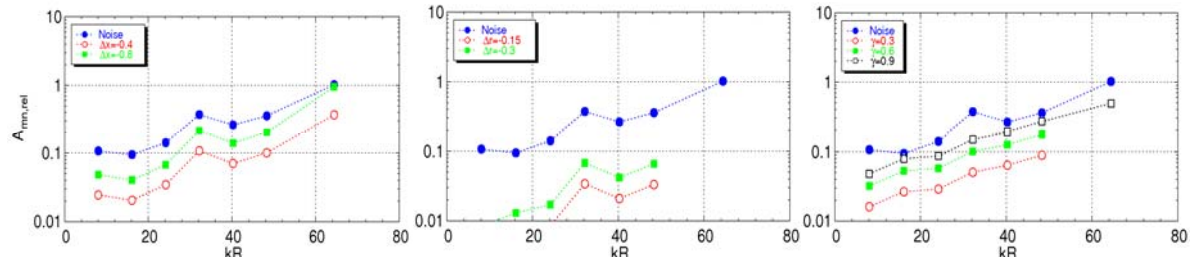

Fig. 17: Impact of different sensor rake installation tolerances on overall accuracy of radial mode decomposition (from left to right: rake axial offset Δx, rake radial offset Δr, rake shaft rotation γ)

VIII. Superposition of aerodynamic modes

An important issue to clarify was to which extent the acoustic mode measurement were influenced by the presence of the rotor wakes. This problem was addressed so far only during the analysis of an URANS calculation[7]. Generally a microphone cannot distinguish between acoustic and hydrodynamic pressure perturbations. A first insight gives the contour of pressure fluctuations measured directly at the OGV exit with the RMD1 sensor rakes for the BPF component at 50% shaft speed. The plot is shown in the left of Fig. 18 and clearly exhibits a fine azimuthal structure. An azimuthal mode decomposition reveals four dominant mode orders, i.e. m=-64, m=-22, m=20 and m=62. Since at the given frequency and operating condition only acoustic azimuthal mode orders m=-11, ..., +11 are cut-on, the observed modes must be purely hydrodynamic. They appear at the same orders as are predicted for the acoustic blade row interactions according to Tyler and Sofrin[10]. Azimuthal mode analysis results are shown in the same diagram for three different radial rake positions: r=1 being closest to the outer duct wall, r=5 in the mid height of the duct and r=10 the second closest station to the hub. Obviously the hydrodynamic modes are stronger close to the hub.

Fig. 19 shows the pressure map of the same frequency component and operating point measured by RMD2 rakes further downstream. A large part of the high-order perturbations vanished. Main contributions of the hydrodynamic modes seem to exist close to hub, which is confirmed by the azimuthal mode analysis results showing large amplitudes for modes m=-22 and m=20 at radial position n_r=10. Close to the outer duct wall mainly mode m=-22 and in the middle of the duct no significant mode could be observed. Interesting is the comparison with the RMD3 measurement at the outer duct wall: here no hydrodynamic mode was visible at all, which might be explained by higher dissipation rates in the duct boundary layer compared to the flow field inside the duct.

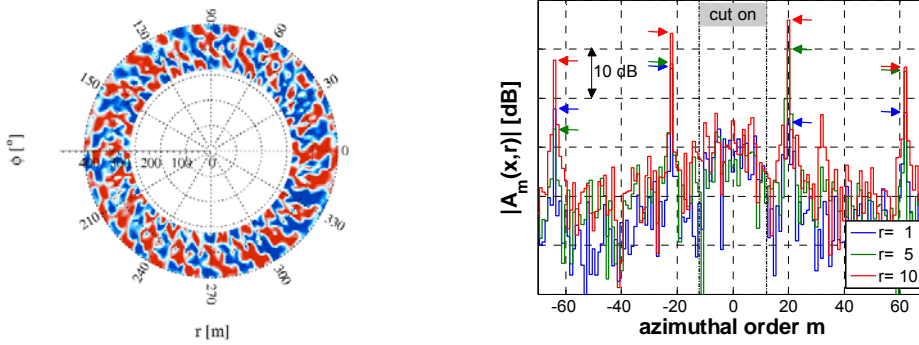American Institute of Aeronautics and Astronautics

Fig. 18: Left: Pressure fluctuations measured by RMD1 sensor rakes at OGV exit (first axial measurement plane) for BPF component at 50% shaft speed. Right: Result of azimuthal mode decomposition at radial station r=1 (close to duct wall), at r=5 (mid radial height) and at r=10 (close to hub wall).
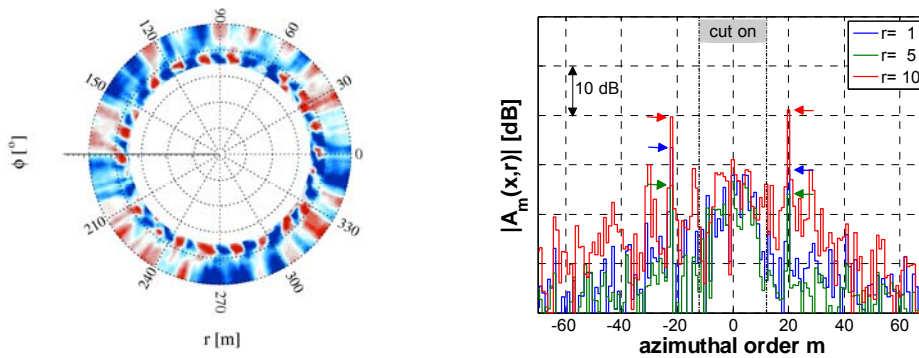

Fig. 19: Same as Fig. 18 but for RMD2 sensor rakes at nozzle equivalent plane (first axial measurement plane).
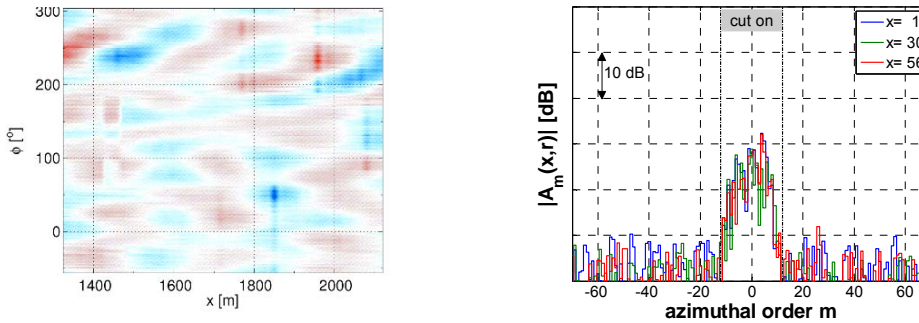

Fig. 20: Same as Fig. 18 but for RMD3 wall-mounted sensor array at nozzle equivalent plane.

A different picture results at higher shaft speeds. As can be verified in Fig. 21, at 100% shaft speed the pressure distribution of the BPF component now comprises high mode amplitudes at RMD2 plane for all dominant rotor-stator interaction mode orders. But in contrast to the measurements at 50% shaft speed, in this case the mode orders m=20 and m=-22 are strongest in the middle of the duct and slightly weaker in direction to the duct walls. Since at the given operating point acoustic mode orders m=-25, …, +25 were cut-on, it is doubtable whether both mode orders are of aerodynamic or acoustic nature. However, directly at the outer duct wall again no dominant modes were detected, see Fig. 22, which leads to the assumption that all modes measured at RMD2 are again purely aerodynamic perturbations.

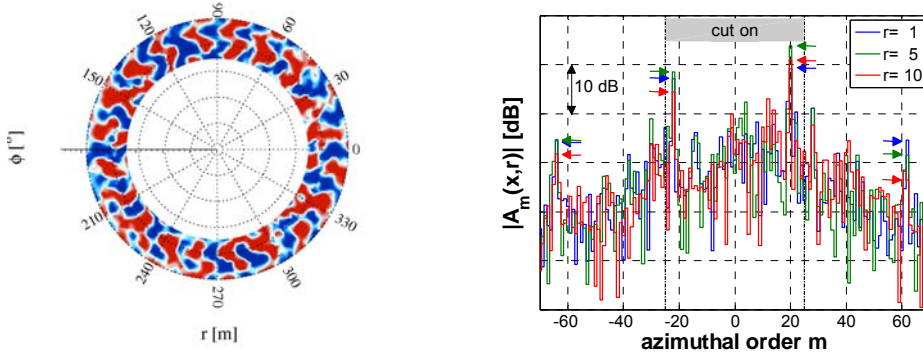American Institute of Aeronautics and Astronautics

Fig. 21: Left: Pressure fluctuations measured by RMD2 sensor rakes for BPF component at 100% shaft speed. Right: Result of azimuthal mode decomposition at radial stations r=1 (close to duct wall), at r=5 (mid radial height) and at r=10 (close to hub wall).
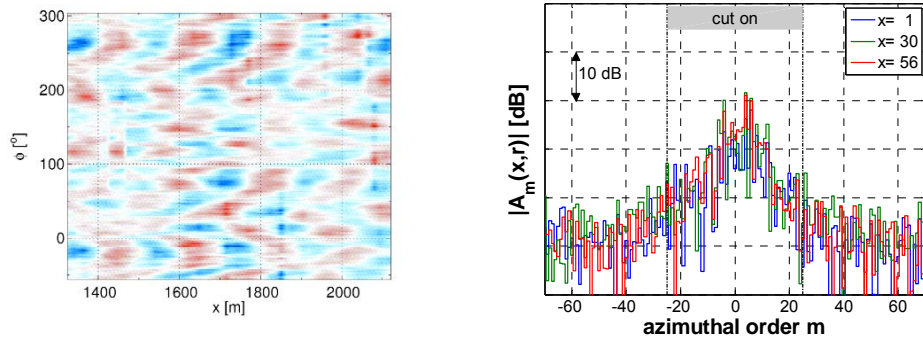

Fig. 22: Same Fig. 21 but for RMD3 wall-mounted sensor array at nozzle equivalent plane.

With the purpose to investigate – and if possible to separate – the influence on the radial mode decomposition the acoustic model matrix **W** was extended by an aerodynamic part. In the extended model the circumferential and radial mode shapes of the aerodynamic perturbations are described by the same eigenfunctions as for the corresponding acoustic modes, but the axial wave numbers are replaced by an aerodynamic wave number

$$k^h = \frac{k}{M_x} \bullet$$
(4)

The basic assumption is that the aerodynamic waves are convected with the mean flow velocity, which here is represented by the mean axial Mach number M_x averaged over the duct cross section. k denotes the wave number under free-field conditions. As pointed out by Weckmüller et al[7], it might be not meaningful to give the aerodynamic modes a physical interpretation, since in a more narrow sense their space-time structure changes while propagating along the duct, which is not the case for acoustic modes under fixed conditions.

In Fig. 23 the effect of the extended mode analysis is demonstrated for the RMD2 rake measurement at 100% shaft speed. The blue curve describes the reference case in which no aerodynamic modes are taken into account. Then the acoustic mode analysis of the pressure field yields a high sound power level for the rotor-stator interaction mode m=20. Striking is the high level of the reflected mode indicating a subnormal quality of the analysis. If aerodynamic modes of radial order n=0 are included, the energy of the interaction mode m=-22 consisting of only a single radial order is well absorbed. Since the amplitude of mode (20,1) is much larger than of mode (20,0), the total sound power of mode order m=20 is almost unchanged. However, the green curve shows a drastic change with inclusion of the next radial order n=1, which results in the complete filtering of mode m=20. The fact that also other downstream propagating azimuthal mode orders are affected by the extended analysis may be linked to the idea that the shape of the rotor wakes varies significantly, i.e. partly flush out, when propagating downstream. Overall, the extended mode analysis produces surprisingly reasonable results in view of the facts, that data for axial wave number analysis was available only at two planes and the aerodynamic model describes only a mean axial convection without radial and circumferential components.

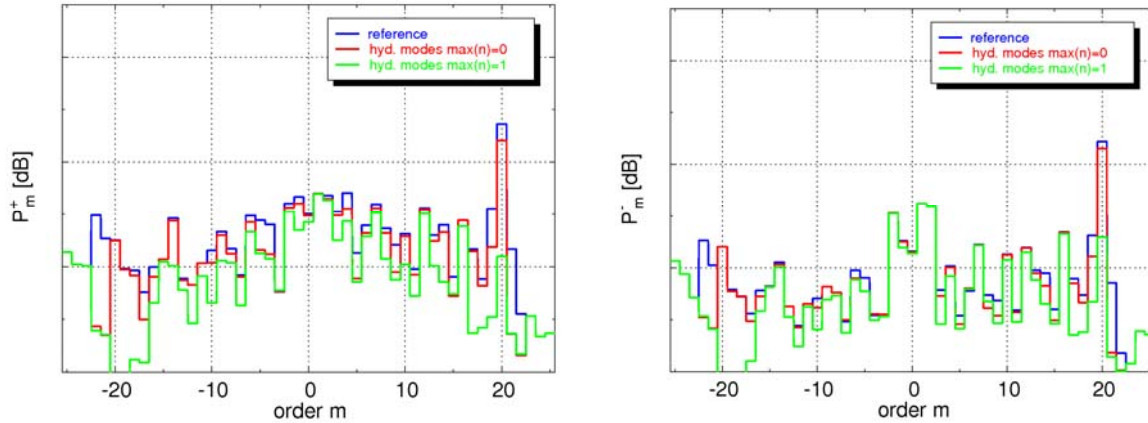American Institute of Aeronautics and Astronautics
092407

Fig. 23: Sound power carried by radial modes of azimuthal order m in and against flow direction. Result of the radial mode analysis without and with consideration of hydrodynamic modes applied for RMD2 sensor rakes, BPF component at 100% shaft speed.

IX.   Comparison of RMD2 and RMD3 results for various operating conditions

In Figures Fig. 24 and Fig. 25 the sound powers transported by the different azimuthal mode orders at 2BPF respectively 3BPF in flow direction are compared for RMD2 and RMD3 and three different shaft speeds. Mode orders that can be related to explicable blade row interactions are labeled accordingly. Overall the spectra obtained by RMD2 and RMD 3 look identical. Indeed in most cases the same dominant mode orders are detected with almost the same power levels. However, as discussed in section VI for the 3BPF component at 80% speed, the distribution of the energy among the radial orders might be slightly different, which is of importance in case the data is used for validation purposes or as input for numerical predictions. Under the assumption that also for 2BPF and 3BPF no aerodynamic modes were detected by array RMD3, the comparison with the RMD2 results allows the conclusion that – in contrast to the BPF component – here also for RMD2 aerodynamic modes are of minor relevance. Reasons for much larger ratios of acoustic to aerodynamic mode amplitudes are the fact that the rotor-stator interaction is acoustically cut-on and the liner efficiency is decreased for 2BPF and 3BPF at higher shaft speeds.

Striking are the higher amplitudes of the reflected modes measured by the RMD2 rakes, compare Fig. 26. An explanation might be upstream reflections at the rake body. Further should be taken into consideration the approximately 2.5 times larger number of RMD3 measurement positions leading to a better compensation of errors.

The good quality and the comparability of the RMD2 and RMD3 results are confirmed in the alternative data representations of Fig. 27 and Fig. 28. Explicitly shown are the sound power levels of all modes that result out of the interaction of rotor/OGV and rotor/ISS with subsequent transmission through the OGV. The sound powers of the dominant modes agree within 1dB to 2dB precision. For the inferior modes most deviations are between 1dB to 6dB. Principally the deviations increase with increasing frequency and number of propagating modes. In general clear trends regarding increase of power levels with increasing shaft speed can be observed. It should be noted that the acoustic liner installed in the bypass duct upstream of the RMD2 and RMD3 devices had two liner spices. Thus it is likely that fractions of modes, which originated from the known blade interaction mechanisms afterwards were scattered at the splices and thus are accumulated in the term 'rest' of the unidentified modes.
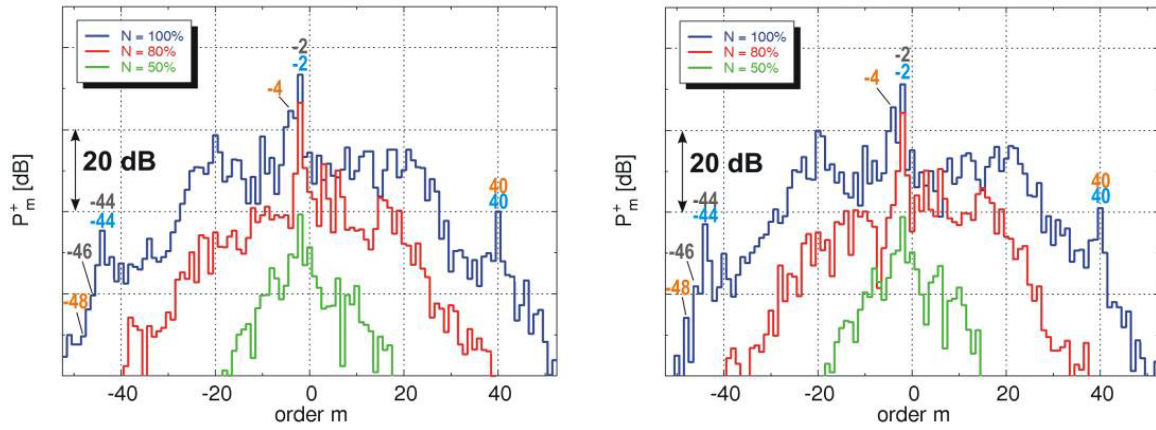
American Institute of Aeronautics and Astronautics

Fig. 24: Sound power carried by radial modes of azimuthal order m in flow direction. Result of the radial mode analysis obtained with RMD2 sensor rakes (left) and RMD3 wall-mounted array (right) for 2BPF component at 50%, 80% and 100% shaft speed.
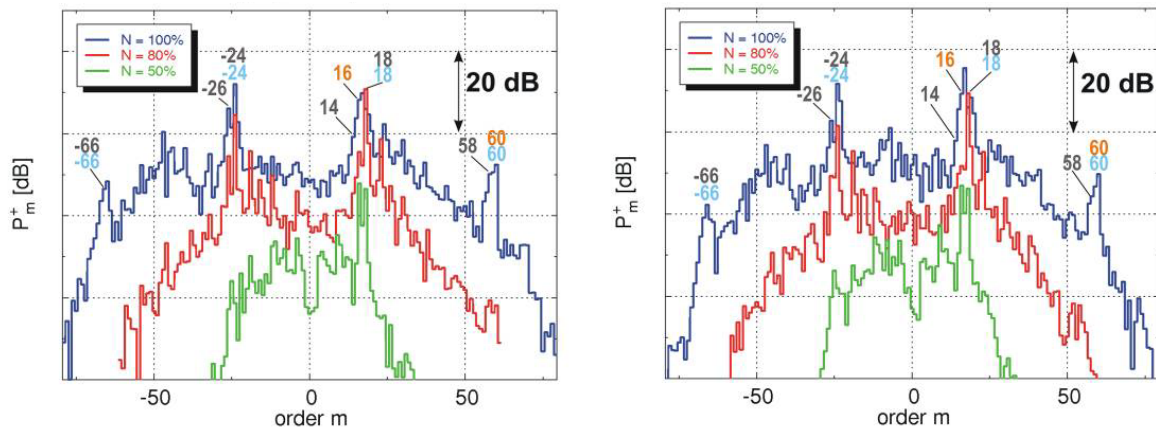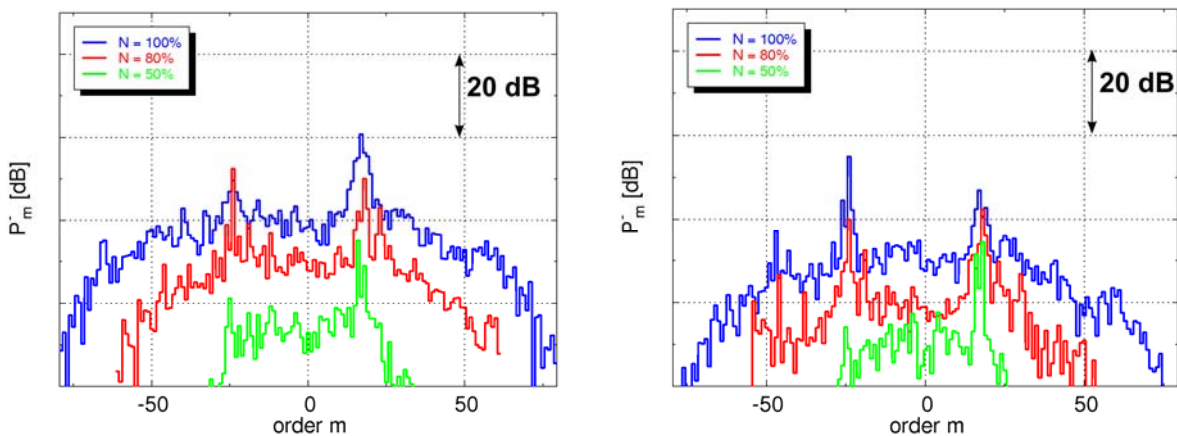

Fig. 25: Same as Fig. 24 but for 3BPF component.

Fig. 26: Same as Fig. 25 but for reflected, i.e. upstream propagating, modes.
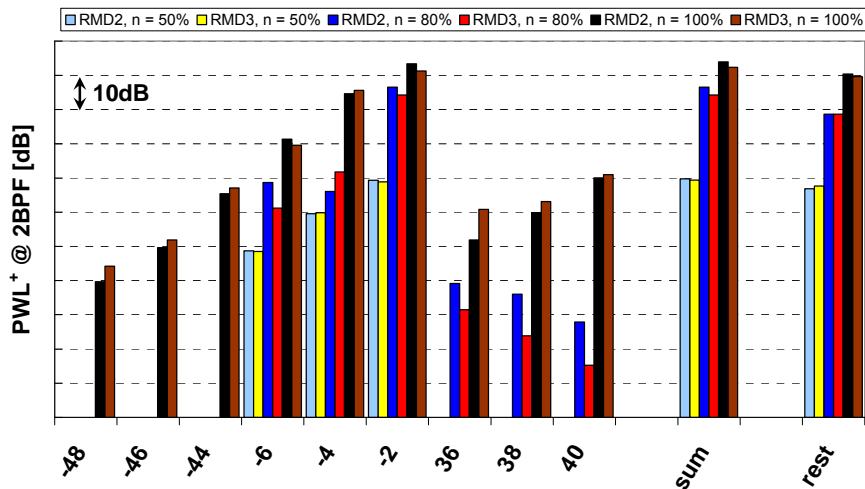
Fig. 27: Comparison of sound powers measured for specific blade row interactions by arrays RMD2 and RMD3 for 2BPF component at 50%, 80% and 100% shaft speed (rotor/ISS modes result out of rotor/ISS interaction and subsequent scattering at the rotor and OGV).*
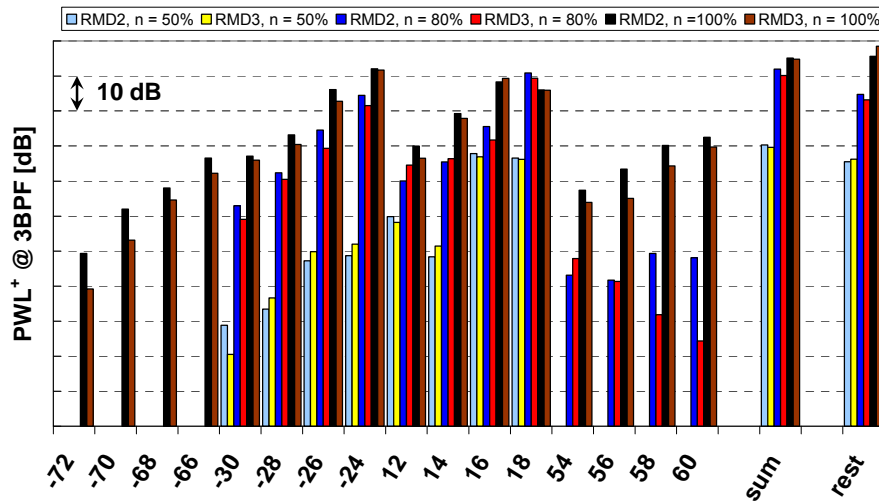

Fig. 28: Same as Fig. 27 but for 3BPF component.

Conclusions and Outlook

Three radial mode detection (RMD) devices were designed for the application at two different locations in the bypass duct of a new modular large scale fan rig test facility. The outcomes of RMD measurements using radial sensor rakes respectively wall-flush mounted arrays of microphones at the outer duct wall were compared at high frequencies up to kR=75. Both arrays were optimised with respect to minimal vulnerability to measurement noise. In general the measured radial mode spectra show a good agreement, small differences are attributed to the specific numerical properties of the inverted model matrices and the different susceptibility to mean flow effects.

The sensor rake measurements were influenced by aerodynamic perturbations originating from the fan rotor wakes also quite a few chord lengths downstream of the OGVs. However, it was shown that the radial mode analysis can be significantly improved when the acoustic modal basis is extended by appropriate aerodynamic eigenfunctions. Further discussed was the sensitivity of sensor rakes against manufacturing and installation

American Institute of Aeronautics and Astronautics
092407

tolerances. In view of the additional complicacies and despite the required length of the instrumented duct section, the application of wall-flush mounted sensor arrays constitutes a good alternative to radial sensor rakes.

In addition to the influence of superposed aerodynamic perturbations, the impact of cut-off modes on the RMD1 analysis close to the OGV exit will be investigated next. Further interesting is the impact of the boundary layer on the mode propagation and the consequences involved for the radial mode decomposition. Future studies will also be related to the analysis of the fan broadband noise components.

Acknowledgements

References

[1] Schwaller, PJG et al., 2004 "Noise Validation of Model Fan Rig with Engine," 12th AIAA/CEAS Aeroacoustics Conf. Cambridge, MA, May 8-10, 2006, Paper AIAA-2006-2479

[2] Tapken, U. und Bauers, R. und Guerin, S. und Enghardt, L.: Radial mode detection of tonal turbofan noise at a modular fan rig facility. Final Workshop of the EU FP 6 Project VITAL (Environmentally friendly aero-engines), 09 - 10 Mar 2009, Budapest, Hungary.

[3] Tapken, U., Enghardt, L., "Optimisation of Sensor Arrays for Radial Mode Analysis in Flow Ducts", 12th AIAA/CEAS Aeroacoustics Conf. Cambridge, MA, May 8-10, 2006, Paper AIAA 2006-2638

[4] Moore, C. Measurement of Radial and Circumferential Modes in Annular and Circular Ducts Journal of Sound and Vibration, 1979, 62, p. 235-256

[5] Heidelberg, L. & Hall, D.: Inlet Acoustic Mode Measurements Using a Continously Rotating Rake, AIAA Journal of Aircraft, 1995, 32, p. 761-767

[6] Enghardt, L.; Zhang, Y. & Neise, W.: Experimental verification of a radial mode analysis technique using wall-flush mounted sensors. Collected Papers from the Joint Meeting "Berlin 99" TU-Berlin, March 14-19, 1999, 137th regular meeting of the Acoustical Society of America, 2nd convention of the EAA: Forum Acusticum - integrating the 25th German Acoustics DAGA Conference; ISBN 3-9804568-5-4, 1999, Paper 3pPA5

[7] Weckmüller, C., Fritzsch, A., and Guérin, S., "Extended Multi-Plane Pressure Mode Matching," Proceedings of the NAG/DAGA 2009 International Conference on Acoustics, Rotterdam, Netherland, March 23-16 2009

[8] Rademaker, E.R.; Sijtsma, P.; Tester, B.J.; Mode detection with an optimized array in a model turbofan engine intake at varying shaft speeds, AIAA Paper 2001-2181, NLR-TP-2001-132, 2001

[9] Mueller D.,Schulz H-J., Zitouni G. and Baumann W., "Europe's Largest Aero Acoustic Test Facility for Aero-Engine Fans - the Development and Operation of the AneCom AeroTest Anechoic Chamber," AIAA-2005-3050, 11th AIAA/CEAS Aeroacoustics Conference, Monterey, 2005

[10] Tyler, J.M., Sofrin, T.G.: "Axial flow compressor noise", SAE Transaction 70, pp- 309-332, 1962.

[11] Morfey, C.L.: "Acoustic energy in non-uniform flows", Journal of Sound and Vibration 14(2), pp. 159-170, 1971.

[12] Nelson, P. and Yoon, S., Estimation of Acoustic Source Strength by Inverse Methods: Part I, Conditioning of the Inverse Problem, Journal of Sound and Vibration, Vol. 233, No. 4, 2000, pp. 643-668.

[13] Kim, Y. and Nelson, P., Optimal Regularisation of Acoustics Source Reconstruction by Inverse Methods, Journal of Sound and Vibration, Vol. 275, No. 3-5, 2004, pp. 463-487.

[14] Tapken, U., Raitor, T., Enghardt, L., "Tonal Noise Radiation from an UHBR Fan – Optimized In-Duct Radial Mode Analysis", 15th AIAA/CEAS Aeroacoustic Conference; 11-13 May 2009, Miami, USA, No. AIAA 2009-3226, 2009.